6

# Blind Detection, Parameters Estimation and Despreading of DS-CDMA Signals in Multirate Multiuser Cognitive Radio Systems

Crépin Nsiala Nzéza[1] and Roland Gautier[2]
[1]*SEGULA Technologies Automotive,*
*Département Recherche et Innovation, Parc d'Activités Pissaloup,*
[2]*Université Européenne de Bretagne,*
*Université de Brest, Lab-STICC UMR CNRS 3192,*
*France*

## 1. Introduction

The design of smart terminals able to detect reachable frequency bands and configure them according to the available channel state information is a major focus of current research. Two main approaches are addressed in the literature: cooperative scenario and blind methods whom transmission parameters are unknown. Blind spectrum sensing and parameters estimation (at the receiver side) may guarantee a more intensive and efficient spectrum use, a higher quality of service and more flexibility in devices self-configuration. This scenario, which can be viewed as a brick of a Cognitive Radio (CR) (Mitola, 2000) is considered throughout this chapter. We consider the more general case of Direct-Sequence (DS) spread spectrum signals in multiuser multirate CDMA systems where spreading sequences may be longer than the duration of a symbol. An easy way to view the multirate CDMA transmission is to consider the variable spreading length (VSL) technique where all users employ sequences with the same chip period. Moreover, the data rate is tied to the length of the spreading code of each user. Many researches aiming at spectrum sensing in cognitive radio context have been proposed, such as blind cyclostationary approaches (Hosseini et al., 2010), SOS approaches (Cheraghi et al., 2010), Student's t-distribution testing problem (Shen et al., 2011). Authors proved that these methods exhibited very good performances in discriminating against noise due to their robustness to the uncertainty in noise power. Nevertheless, they could be computationally complex since they may require significantly long observation time. Several blind approaches (i.e., when the process of recovering data from multiple simultaneously transmitting users without access to any training sequences) have been addressed in the literature (Buzzi et al., 2010; Khodadad, Ganji & Mohammad, 2010; Khodadad, Ganji & Safaei, 2010; Meng et al., 2010; Yu et al., 2011; Zhang et al., 2011). However, most of them require some prior knowledge about users parameters such as signature waveform, processing gain, pseudo-noise code (for a particular group of active users) or chip rate. These parameters may be unknown in a realistic non-cooperative context. Besides, a PARAFAC based method was addressed in (Kibangou & de Almeida, 2010), but in the single user case in a no noisy environment. Furthermore, in multiuser asynchronous systems both problems of blind

despreading and synchronization are much more demanding, what become much more challenging. In this chapter, we addressed an iterative with deflation approach aiming to the blind multiuser multirate signals detection. Moreover, in (Koivisto & Koivunen, 2007), a similar method was proposed starting from that given in (Nsiala Nzéza, 2006), without addressing the multiuser multirate blind detection. Moreover, even though authors in (Koivisto & Koivunen, 2007), analyzing the scheme in (Nsiala Nzéza et al., 2004) claimed that good performances can be obtained in asynchronous multiuser systems, the computing time increases concomitantly with both the number of users and the correlation matrix size. Besides, the number of interfering users in (Koivisto & Koivunen, 2007) is assumed to be known at the receiver side, contrary to what is assumed in this paper. At last, similar methods to those quoted in this chapter were addressed in (Ghavami & Abolhassani, 2008; 2009). Nevertheless, authors do not improve performances, since the multiuser multirate case is was not addressed. Besides, the multiuser synchronization, even with the knowledge of certain parameters is not theoreticaly discussed. Consequently, an alternative method to those quoted above is herein proposed. This efficient and low complexity scheme does not require any prior knowledge about the transmission. The novelty of the proposed approach lies in the use of iterative algorithms combining both deflation and second-order statistical estimators methods. The application in cases of long and short spreading code transmissions is discussed and performances are investigated.

## 2. Signal model and assumption

Let us first consider the single user case, before dealing with both multirate and/or multiuser cases. In all cases, the uplink scenario of a DS-CDMA network is considered. This section also quickly highlights the long sequence signal model even though the application of the proposed method to long sequences case will be shown later in Section 7.

### 2.1 Single user signal model

#### 2.1.1 Short spreading code case

In this case each symbol is spread by a whole spreading code, i.e., $T_s = LT_c$, where $L$, $T_s$ and $T_c$ stand for the spreading sequence gain, the symbol period and the chip period, respectively. The continuous-time single user signal at the transmitter is given by:

$$s(t) = \sum_{k=-\infty}^{+\infty} a(k)\psi(t - kT_s), \tag{1}$$

where $a(k) \notin \mathbf{a}^T = [a(0), \cdots, a(k), \cdots]$ are the transmitted real- or complex valued symbols drawn from a known constellation. $\psi(t)$ stands for the signature waveform which can be expressed as:

$$\psi(t) = \sum_{l=1}^{L} c(l)g(t - lT_c), \tag{2}$$

with $\psi(t) = 0$ for $t \notin [0, LT_c[$, and $c(l) \in \mathbf{c}^T = [c(0), \cdots, c(l), \cdots]$ being the $l^{th}$ chip of the spreading sequence and $g(t)$ is the impulse response of the pulse shaping filter. Recall that the same spreading code is repeated for every symbol, i.e., the system is a short-code DS-CDMA system. The signal is modulated to carrier frequency $f_c$, i.e., mixed with carrier

$\sqrt{2A'}e^{j(2\pi t f_c+\phi')}$, where $A'$ and $\phi'$ are the power and phase. The signal is transmitted through a flat-fading channel. The received continuous-time signal can be written as:

$$y(t) = \sum_{p=1}^{P} s(t - T_p - T_d)\sqrt{2A}e^{j(2\pi t f_c+\phi)} + b(t), \tag{3}$$

where $T_p$ is the channel propagation delay relative to the beginning of each symbol interval, $T_d$ is the signal delay at the receiver side, $A = \mathcal{G}_p A'$ is the received power ($\mathcal{G}_p$ is the path fading factor), $\phi = \phi' - 2\pi f_c T_p$ is the phase offset and $b(t)$ is additive white Gaussian noise of variance $\sigma_b^2$, $P$ is the number of channel taps. Equation 3 may then be expressed in a close-form as:

$$y(t) = \sum_{k=-\infty}^{+\infty} a(k)h(t - kT_s - T_d) + b(t), \tag{4}$$

where $h(t) = \sum_{p=1}^{P} \sqrt{2A}e^{j(2\pi t f_c+\phi)}\psi(t - T_p)$. Accordingly, following assumptions are made: $a(k)$ are independent, centered with variance $\sigma_a^2$; both $T_p$ and $T_d$ are supposed to be constant during the observation time and to satisfy $0 \leqslant T_p < T_d < T_s$; and the signal-to-noise ratio (SNR in dB) at the detector input may be negative (signal hidden in the noise).

### 2.1.2 Long spreading code signal model

Without loss of generality, the base-band transmission in an AWGN channel is first considered. In this case, $h(t)$ can be rewritten as $h(t) = \psi(t) = \sum_{l=1}^{L} c(l)g(t - lT_c)$. Moreover, in a long spreading code approach, a whole code spread $Q_s$ ($Q_s \in \mathbb{N}^*$) consecutive symbols. Therefore, each symbol can be viewed as spread by a code of length $L_s = \frac{L}{Q_s}$ (i.e., $T_s = L_s T_c$). Let us also define $\psi_s(t)$ as $\psi_s(t) = 0$ for $t \notin [0, L_s T_c[$. Hence, Equation 4 becomes:

$$y(t) = \sum_{k=-\infty}^{+\infty} a(k)\psi_s(t - kT_s - T_d) + b(t), \tag{5}$$

where $\psi_s(t) = \sum_{l=(\langle k\rangle_{Q_s})L_s}^{(\langle k+1\rangle_{Q_s})L_s-1} c(l)g_s(t - lT_c)$, $\langle x\rangle \equiv x \ modulo \ Q_s$. First, setting $L_s$=$L$ and $Q_s$=1 leads to the short spreading code case, i.e.,

$$y(t) = \sum_{k=-\infty}^{+\infty} a(k)\psi(t - kT_s - T_d) + b(t). \tag{6}$$

Secondly, by setting $h_s(t) = \sum_{p=1}^{P} \sqrt{2A}e^{j(2\pi t f_c+\phi)}\psi_s(t - T_p)$, Equation 5 can be expressed as Equation 4, taking into account $P$ channels taps as:

$$y(t) = \sum_{k=-\infty}^{+\infty} a(k)h_s(t - kT_s - T_d) + b(t). \tag{7}$$

Furthermore, setting $L_s$=$L$, Equation 7 leads to a similar expression than in Equation 4. Therefore, in the sequel, only the short spreading code will be considered for multiuser signal model. However, when the long spreading code case will be discussed, there will be a special indication.

### 2.2 Multiuser multirate signal model

The VSL-based asynchronous DS-CDMA system where $\{R_0, R_1, \cdots, R_{S-1}\}$ stands for a set of $S$ available data rates is considered. A different slow fading multipath channel with i.i.d Rayleigh random variables and unity second moment fading amplitudes is assumed for each interfering user. Let us set $N_u^i$ the number of active users transmitting at $R_i$ (hence, belonging to group $i$) and $N_u$ the total number of users such that $\sum_{i=0}^{S-1} N_u^i = N_u$. The $n^{th}$ transmitted signal at $R_i$, denoted throughout this chapter as the $(n,i)^{th}$ user, is written as:

$$s_{n,i}(t) = \sum_{k=-\infty}^{+\infty} a_{n,i}(k)\psi_{n,i}(t - kT_{s,i}), \tag{8}$$

where $\psi_{n,i}(t) = \sum_{l=1}^{L_i} c_{n,i}(l)g_i(t - lT_c)$ represents the $(n,i)^{th}$ user's signature code, i.e., the convolution of the transmission filter with the spreading sequence $\{c_{n,i}(l)\}_{l=1\cdots L_i}\}$ chipping pulse. $L_i$ is the spreading factor for the $(n,i)^{th}$ user or for the $n^{th}$ transmitted signal at $R_i$,i.e., with the symbol rate $T_{s,i}$. Moreover, let us assume that the channel seen by users in group $i$ is different from that seen by ones in another group, but with the same number $P$ of paths. $\mathcal{G}_{p,i}$ and $T_{p,i}$ represent the $p^{th}$ path fading factor and its corresponding transmission delay which typically satifies: $0 \leq T_{p,i} \leq< T_{d_{n,i}} < T_{s_i}$. The $(n,i)^{th}$ user channel corrupted received signal is done by:

$$y_{n,i}(t) = \sum_{k=-\infty}^{+\infty} a_{n,i}(k)h_{n,i}(t - kT_{s,i} - T_{d_{n,i}}) + b(t), \tag{9}$$

where $h_{n,i}(t) = \sum_{p=0}^{P-1} \sqrt{2A_i}e^{j(2\pi t f_c + \phi_i)}\psi_{n,i}(t - T_{p,i})$, $A_i$ and $\phi_i$ are defined as for Equation 3 using $\mathcal{G}_{p,i}$, $T_{d_{n,i}}$ stands for the $(n,i)^{th}$ user's delay at the reciver side, which satifies: $T_{d_{n,i}} < T_{s_i}$. In Equation 9, it was assumed that users in group $i$ are transmitted with the same power in order to further simplify theoretical analysis. However it is not required in practise with respect to iterative implementation discussed in Section 6. Concluding for Equation 9, the channel corrupted multiuser signal may be modelled as:

$$y(t) = \sum_{i=0}^{S-1} \sum_{n=0}^{N_u^i - 1} \sum_{k=-\infty}^{+\infty} a_{n,i}(k)h_{n,i}(t - kT_{s_i} - T_{d_{n,i}}) + b(t). \tag{10}$$

Also, using Equations 5 and 10, the long code multiuser multirate signal model may be written as:

$$y(t) = \sum_{i=0}^{S-1} \sum_{n=0}^{N_u^i - 1} \sum_{k=-\infty}^{+\infty} a_{n,i}(k)h_{s_{n,i}}(t - kT_{s_i} - T_{d_{n,i}}) + b(t). \tag{11}$$

## 3. Description of the proposed approach

Fig. 1 shows the different steps of the proposed approach in a sequential manner for getting the full picture of the subject. Since we focus on the last three steps in this chapter, the spectrum sensing step may be considered as a preliminary one, hence it will be assumed in what follows that this step has been performed. Even so, the reader will find details in (Nzéza et al., 2009) about the proposed method for this purpose. Spectral components (e.g., central frequency bandwidth) are estimated by the averaged periodogram non-parametric approach using a Fast Fourier Transform (FFT) combined with a detection threshold. This

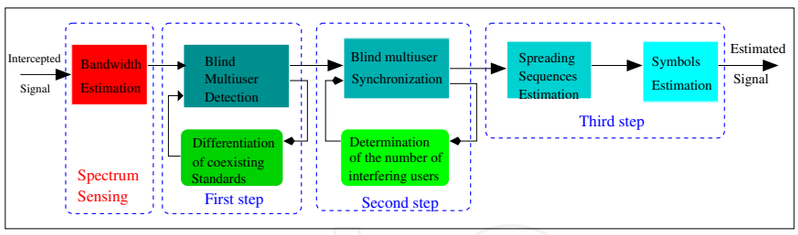


Fig. 1. Illustration of different stages of the proposed method (after the bandwidth estimation process).

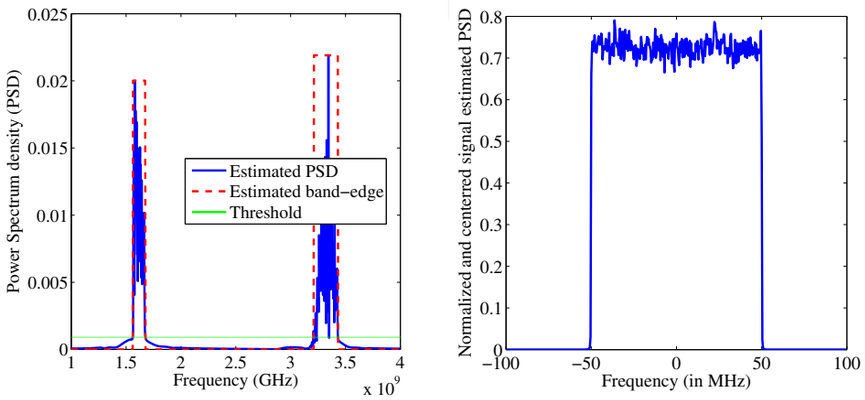


(a) Filtered periodogram with the estimated threshold

(b) Estimaton of the bandwidth @1.62 GHz

Fig. 2. Blind bandwidth estimation and center frequencies recovering.

threshold is computed from the signal received power estimation as shown on Fig. 2 (a), obtained with following parameters: One signal at 1.62 $GHz$ and another at 3.3 $GHz$, spread with complex GOLD sequences with $L$=127, $T_c$=150 $MHz$, $F_e$=300 $MHz$, $T_F$=2$\mu s$, $K$=300, $QPSK$ modulation, COST207RAx6 (Committee, 1989) channel, and the SNR $= -3$ dB at the receiver side. If we are interested by the signal at 1.62 $GHz$, we deduct a frequency-band of $\widetilde{W}$=100 $MHz$, as evidenced on Fig. 2 (b). Note that if two or more signals share the same bandwidth, their differenciation is performed through the blind detection step, which is the first one on Fig. 1.

The first steps allows to detect signals and to estimate their data rate through the analysis of fluctuations of correlation estimators (Nsiala Nzéza, 2006) whithin each identified bandwidth of interest. Besides, it allows a multi-standard detection through a differentiation of various standards data rate as suggested in (Williams et al., 2004). Successive investigations of the contributions of noise and channel-corrupted signal through the analysis of the second-order moment of the correlation estimator computed from many randomly-selected analysis windows constitutes the key point of the proposed temporal parameters estimation approach. As a result, we compute a function which is a measurement of these fluctuations. The obtained curve highlights equispaced peaks of different amplitudes, therefore for different symbol periods which leads to a low computational complexity and an efficient estimation of symbols duration. The proposed scheme is also insensitive to phase and frequency offsets since it is the square modulus which is computed.

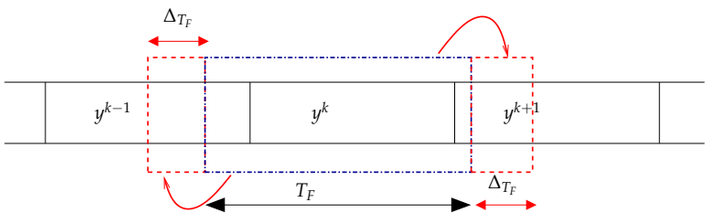


Fig. 3. Correlation computation over an analysis window.

The knowledge of symbol durations permits to perform the synchronization process. This constitutes the second step as highlighted on Fig. 1. Moreover, through the analysis of correlation matrix at this stage, the synchronization may be done iteratively by deflation using, as appropriate, one of the criteria detailed in Sections 4 and 5. This process also allows to determine the number of interfering users transmitting at the same data rate by determinating the number of the synchronization peaks. Finally, in the third step on Fig. 1, codes and symbols are recovered even at very low SNR using linear algebra techniques, also described in Sections 4 and 5. The assessment of those parameters constitues a brick of a CR's receiver and allows its self-reconfigurability. It is very important to note that although the overall method is presented sequentially, it must be implemented iteratively, as discussed in Section 6, and further applied to long spreading codes case in Section 7.

## 4. Application to short spreading codes in the single user case

### 4.1 Estimation of the symbol duration

The analysis of the autocorrelation fluctuations estimators allows to achieve a direct blind signals detection and standards differentiation. The estimation process of the symbol duration $T_s$ uses correlation properties of the received signal. Using $K$ temporal windows of duration $T_F$, an autocorrelation estimation $\widehat{R}^k_{yy}$ of the received signal can be written as:

$$\widehat{R}^k_{yy}(\theta) = \frac{1}{T_F + 2\Delta_{T_F}} \int_{-\Delta_{T_F}}^{T_F+\Delta_{T_F}} y^k(t)(y^k)^*(t-\theta)dt, \tag{12}$$

where $y^k(t)$ is the signal sample over the $k^{th}$ window and $(\cdot)^*$ denotes the conjugate transpose of $(\cdot)$. In order to avoid edge effects, $\widehat{R}^k_{yy}$ is computed within each window $k$ and also during $\Delta_{T_F}$ at both right and left side of the $k^{th}$ window, as illustrated on Fig. 3. Equation 12 constitutes the main key of the detection algorithm, since it reduces constraints on the window duration $T_F$, and thus on the total number $K$ of analysis windows. $\Delta_{T_F}$ can be theoretically neglicted compared to $T_F$ ($\frac{T_F}{4} \leq \Delta_{T_F} \leq \frac{T_F}{2}$), since Equation 12 is computed from many analysis windows. However, it is necessary to calculate it in this manner in order to avoid edge effects. Without loss of generality, Equation 12 can be reexpressed more simply for further theoretical analysis as:

$$\widehat{R}^k_{yy}(\theta) = \frac{1}{T_F} \int_0^{T_F} y^k(t)(y^k)^*(t-\theta)dt. \tag{13}$$

Moreover, from simulations results, which will be discussed later, the condition $\frac{T_F}{4} \leq \Delta_{T_F} \leq \frac{T_F}{4}$ seems to be a good choice of $\Delta_{T_F}$. $\widehat{R}_{yy}(\theta)$ is computed over $K$ windows, and its second-order

moment is given by:

$$\widehat{\mathcal{E}}\left\{|\widehat{R}_{yy}(\theta)|^2\right\} = \frac{1}{K}\sum_{k=0}^{K-1}|\widehat{R}^k_{yy}(\theta)|^2 = \Phi(\theta), \tag{14}$$

where $\widehat{\mathcal{E}}(\cdot)$ is the estimated expectation of $(\cdot)$. Hence, $\Phi(\theta)$ is a measurement of the fluctuations of $\widehat{R}_{yy}(\theta)$, as proved in the sequel. Note that it is assumed an average $\mu_{\widehat{R}_{yy}}(\theta)=\mathcal{E}\left\{|\widehat{R}_{yy}(\theta)|\right\}=0$ in Equation 14 for theoretical analysis. In practise, $\Phi(\theta)$ may be computed as:

$$\Phi(\theta) = \widehat{\mathcal{E}}\left\{|\widehat{R}_{yy}(\theta)|^2 - |\mu_{\widehat{R}_{yy}}(\theta)|^2\right\}. \tag{15}$$

Equation 15 represents the centered second order moment of the magnitude of the correlation fluctuations or variance. However, since fluctuations are computed from many randomly-selected windows, Equation 14 is more suitable for theoretical purpose. The difference between both Equations 15 and 14 lies in the magnitude of fluctuations peaks. With assumptions made in Section 2, we have:

$$\widehat{R}_{yy}(\theta) \simeq \widehat{R}_{ss}(\theta) + \widehat{R}_{bb}(\theta), \tag{16}$$

where $\widehat{R}_{ss}(\theta)$ and $\widehat{R}_{bb}(\theta)$ are the estimates of the noise-free signal $s(t)$ and that of the noise autocorrelation fluctuations, respectively. Since symbols are assumed to be independent, uncorrelated with the noise, the variance of $\widehat{R}_{yy}(\theta)$ using Equation 14 is done by:

$$\Phi(\theta) = \Phi_s(\theta) + \Phi_b(\theta), \tag{17}$$

where $\Phi_s(\theta)$ and $\Phi_b(\theta)$ stand for the fluctuations due to the noise-free signal and that due to the additive random-noise, respectively. Expression 17 proves that $\Phi(\theta)$ is a measurement of the variations of the estimator of autocorrelation fluctuations. Since fluctuations are computed from many randomly-selected windows, they do not depend on the signal relative delay, nor on channel path delays. Channel gains act as a multiplicative factor in the fluctuations curve, as it will be shown hereinafter.

#### 4.1.1 Noise contribution to global fluctuations $\Phi(\theta)$

Assume a receiver filter with a flat frequency response in $[-W/2, +W/2]$ and null outside. As proved in (Nsiala Nzéza, 2006), fluctuations $\Phi_b(\theta)$ are uniformly distributed over all values of $\theta$. Hence, they can be characterized by their mean $m_{\Phi_b}$ and standard deviation $\sigma_{\Phi_b}$ as:

$$m_{\Phi_b} = \frac{\sigma_b^4}{WT_F} \quad \text{(a)}, \; \sigma_{\Phi_b} = \sqrt{\frac{2}{K}}\frac{\sigma_b^4}{WT_F} \quad \text{(b)}. \tag{18}$$

Equation 18 (b) shows that increasing the number $K$ of windows improves the detection by lowering noise contribution.

#### 4.1.2 Signal contribution to global fluctuations $\Phi(\theta)$

By only considering the noise-free signal, we demonstrate in (Nsiala Nzéza, 2006) that on average, high amplitudes of its fluctuations, set to as $\Phi_s(\theta)$, occur for $\theta$ multiple of $T_s$. Then,

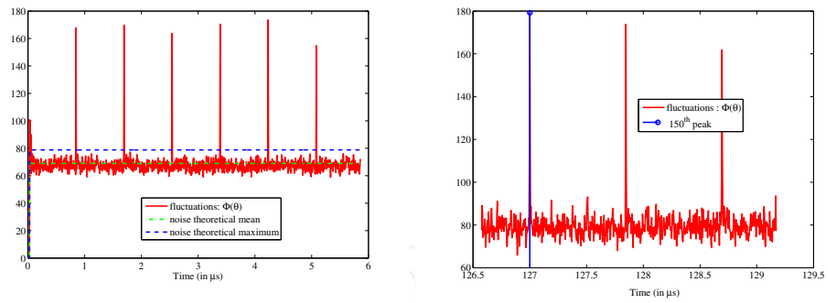


(a) Fluctuations $\Phi(\theta)$ (b) Estimation of $\widetilde{T}_s$

Fig. 4. Estimation of the symbol period through fluctuations $\Phi(\theta)$ analysis , SNR $= -7$ dB in uplink.

for each $\theta$ multiple of $T_s$, both fluctuations average amplitude $m_{\Phi_s}$ and standard deviation $\sigma_{\Phi_s}$ are given by:

$$m_{\Phi_s} = \frac{T_s}{T_F}\widetilde{\sigma}_s^4 = \frac{LT_c}{T_F}\widetilde{\sigma}_s^4, \text{ and } \sigma_{\Phi_s} = \sqrt{\frac{2}{K}}m_{\Phi_s} = \sqrt{\frac{2}{K}}\frac{T_s}{T_F}\widetilde{\sigma}_s^4, \tag{19}$$

where $\widetilde{\sigma}_s^2$ stands for the channel-corrupted signal power at the receiver side. Equation 19 shows that the fluctuations curve will exhibit equispaced peaks which average spacing correspond to the estimated symbol period, which allows at itself to do standards differentiation, as illustrated in Fig. 4.
Fig. 4 was obtained with following simulations parameters: Complex GOLD sequence with $L$=127, $T_c$=100 $MHz$, $F_e$=300 $MHz$, $T_F$=2$\mu s$, $K$=300, $QPSK$ modulation, COST207RAx6 Committee (1989) channel, and the SNR $= -7$ dB at the receiver side. Equation 19 also indicates that the average fluctuations amplitude is tied to the sequence length and the signal power at the receiver side. Continuing with Equation 18, a theoretical detection threshold is taken as: $\zeta = m_{\Phi_b} + 3 \cdot \sigma_{\Phi_b}$. This equation shows that, whenever a spread spectrum signal is hidden in the noise, the average of the curve deviates from the theoretical average. Especially, the curve maximum is above the noise fluctuations theoretical maximum. It is precisely this curve behaviour which allows hidden signals detection. The reader may find extra detailed theoretical performance analysis of this blind detection scheme in (Nzéza et al., 2008).

### 4.2 Synchronization process analysis

At this point, only $T_s$ is known. The signal is sampled and divided into $N$ non-overlapping temporal windows of duration $T_F = T_s = MT_e$, $M \in \mathbb{N}^\star$, where $T_e$ is the sampling period. Thus, each window contains $M$ samples. Sampling and chip periods are not equals, and the number of samples per window is not equal to the code length, since these parameters are unknown. From the sampled-received signal vector $\mathbf{y}^e(t)=[s(t), s(t+T_e), \cdots, s(t+(M-1)T_e)]$, the $(M \times N)$-matrix $\mathbf{Y}^e$, which $N$ columns contain $M$ signal samples is computed as:

$$\mathbf{Y}^e = \begin{pmatrix} s(t) & \cdots & s(t+(N-1)T_s) \\ \vdots & \cdots & \vdots \\ s(t+T_s-T_e) & \cdots & s(t+NT_s-T_e) \end{pmatrix}. \tag{20}$$

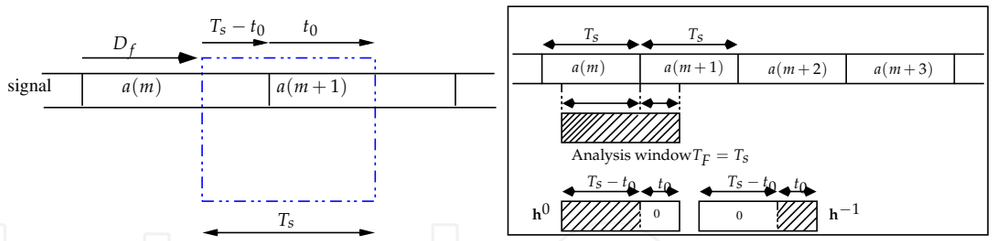


(a) Windows position influence (b) Vectors $\mathbf{h}^0$ and $\mathbf{h}^{-1}$ computation

Fig. 5. Relative position of signals and an analysis window before the synchronization process in uplink.

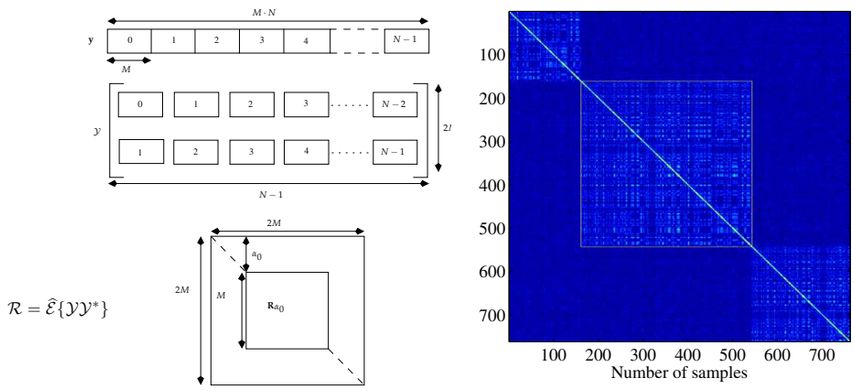


(a) Vector $\mathcal{Y}$ and matrix $\mathcal{R}$ computation (b) Computation of the matrix $\mathcal{R}$

Fig. 6. Double-size correlation matrix estimation with $\widetilde{T_s}$, SNR $= -7$ dB in uplink.

Let us analyze Fig. 5 (a) where $D_f$ and $t_0$ stand for analysis window shifts (here, from left towards right) and the temporal shift between the analysis window and the beginning of a whole symbol, respectively. It clearly appears that any shift $D_f$ induces $t_0$ changes, as well as in Equation 20. As proved in (Nsiala Nzéza, 2006), since the filter $h(t)$ is defined in $[0 \quad T_s[$, Equation 20 can be rewritten as:

$$\mathbf{Y}^e = \left(\mathbf{h}^0 + \mathbf{h}^{-1}\right)\mathbf{a}^T + \mathbf{b}^e, \tag{21}$$

where vector $\mathbf{a}^T = [\cdots, a(m)\cdots]$ contains all symbols, and vectors $\mathbf{h}^0$ and $\mathbf{h}^{-1}$ are defined as follows: $\mathbf{h}^{-1}$ contains the end of the corresponding spreading waveform convolved with the channel during $T_s - t_0$, followed by zeros during $t_0$, meanwhile $\mathbf{h}^0$ contains zeros during $t_0$, followed by the beginning of the corresponding spreading waveform convolved with the channel during $T_s - t_0$, as illustrated on Fig. 5 (b). In Equation 21, $\mathbf{b}^e$ stands for the noise $(M \times N)$-matrix, the received signal $(M \times M)$ correlation matrix $\mathbf{R}$ may be computed as : $\mathbf{R} = \widehat{\mathcal{E}}\{\mathbf{Y}^e(\mathbf{Y}^e)^*\}$. In practise, in order to reduce the computational time, we compute the double size matrix $\mathcal{R} \in \mathbb{C}^{2M\times 2M}$ containing the matrix $\mathbf{R}$ induced by the shift $t_0$, as shown on Fig. 6 (a). Fig. 6 (b) highlights the matrix $\mathcal{R}$ in simultation with the same parameters than on Fig. 4. Moreover, let us assume the signal energy ($\backsimeq T_e\|\mathbf{h}\|^2$ ) uniformly distributed over a period symbol; we obtain the following approximation which is statistically valid if the code

length is large enough (practically it is):

$$\|\mathbf{h}^0\|^2 \backsimeq (1-\alpha_0)\,\|\mathbf{h}\|^2, \quad \text{and} \quad \|\mathbf{h}^{-1}\|^2 \backsimeq \alpha_0\|\mathbf{h}\|^2, \tag{22}$$

where $\alpha_0 = \frac{t_0}{T_s}$. Hence, the estimated correlation matrix can be written as:

$$\mathbf{R} = \sigma_b^2 \left\{ \beta \left\{ (1-\alpha_0)\mathbf{v}^0(\mathbf{v}^0)^* + \alpha_0 \mathbf{v}^{-1}(\mathbf{v}^{-1})^* \right\} + \mathbf{I} \right\}, \tag{23}$$

where $\beta = \rho\frac{T_s}{T_e}$, $\rho$ stands for the signal-to-noise and interference ratio (SNIR), $\mathbf{v}^0$ and $\mathbf{v}^{-1}$ are normalized vectors of $\mathbf{h}^0$ and $\mathbf{h}^{-1}$, and $\mathbf{I}$ is the identity matrix. From Equation 23, an eigenvalue decomposition highlights 2 eigenvalues associated to the signal space and $M-2$ others associated to the noise space (all are assumed to be equal on average to the noise power). Since sequences are supposed uncorrelated, the eigenvalues in an unspecified order are:

$$\lambda_1^0 = \sigma_b^2\left\{\beta\,(1-\alpha_0)+1\right\}, \quad \lambda_2^{-1} = \sigma_b^2\left\{\beta\alpha_0+1\right\}, \quad \lambda_m = \sigma_b^2, \quad m = 2,\cdots,M. \tag{24}$$

The synchronization consists in adjusting more precisely the symbol period by estimating the beginning of the first whole symbol. It is obvious to check that the eigenvalues sum is constant (with a concentration around certain values), and especially does not depend on $\alpha_0$. Therefore, the suitable criterion in order to highlight the phenomenon of concentration is the sum of squares. The FROBENIUS square norm (FSN) of Equation 23 is defined as the sum of the square eigenvalues of Equation 24. Then, after simplifications, we get:

$$\|\mathbf{R}\|^2 = \sigma_b^4\left\{\left(1+2\beta-\beta^2\right)+M\right\} + 2\beta^2\sigma_b^4\left\{1-\alpha_0+\alpha_0^2\right\}. \tag{25}$$

Simplified Equation 25 proves that the sum of square eigenvalues is not sensitive to neither transmission delays nor shifts. The FSN-based (FSNB) criterion is defined as being the constant part of Equation 25, set to $F$:

$$F(\alpha_0) = 1 + \left(\alpha_0^2 - \alpha_0\right). \tag{26}$$

Maximizing the FSN of $\mathbf{R}$ is equivalent in determining the maxima of $F$ (synchronization peak). From Equation 26, $F$ is a convex quadratic function of $\alpha_0$ over $[0,\ 1[$, since there is a periodicity on relative normalized positions $d_f = \frac{D_f}{T_s}$ of an analysis window and that of the signal as highlighted in Fig. 5 (a) and demonstrated in (Nsiala Nzéza, 2006)[pp. 88-115]. By setting $\langle x\rangle \equiv\ x\ modulo\ 1$, $x \in \mathbb{R}$, $\tau = \frac{T_d}{T_s}$ leads to $\alpha_0 = \langle d_f - \tau\rangle$. Consequently, since the delay $\tau$ is assumed constant, Equation 26 only depends on shifts $d_f$:

$$F(d_f) = 1 + \{\langle d_f-\tau\rangle^2 - \langle d_f-\tau\rangle\}. \tag{27}$$

Resulting in a maxima of $F$ obtained for $d_f = \tau \Longrightarrow \alpha_0 = 0$, as shown on Fig. 7 (a). Once the signal is synchronized, the sequence identification process can be performed with the extracted matrix $\mathbf{R}_{\alpha_0}$, as illustrated in Fig. 7 (b).

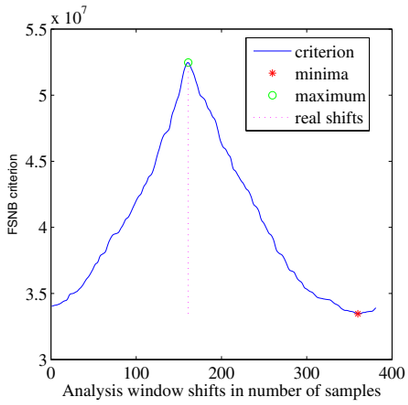


(a) FSNB criterion $F$

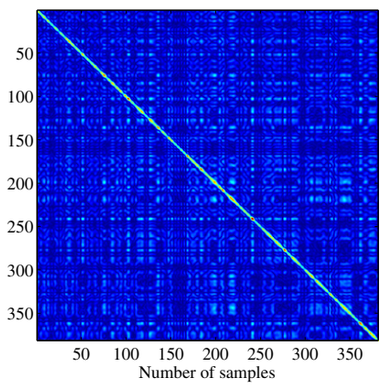


(b) Extracted matrix $\mathbf{R}_{\alpha_0}$

Fig. 7. Synchronization criterion and extracted matrix $\mathbf{R}_{\alpha_0}$, SNR $= -7$ dB in uplink.

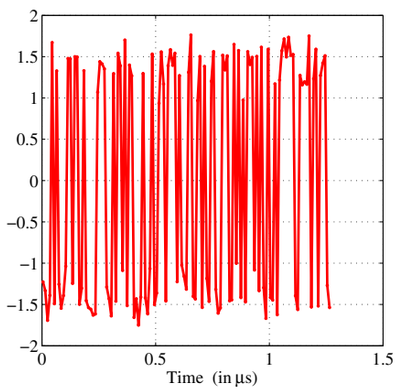


(a) Real part of the code

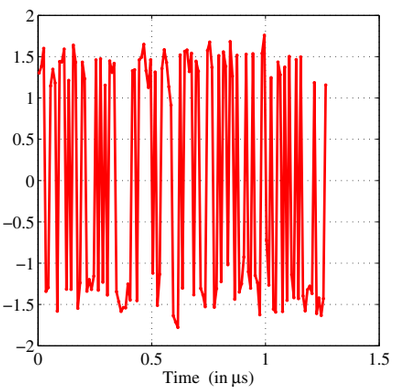


(b) Imaginary part of the code

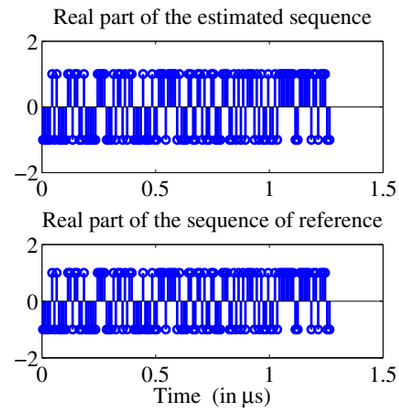


(c) Real binary part of the code

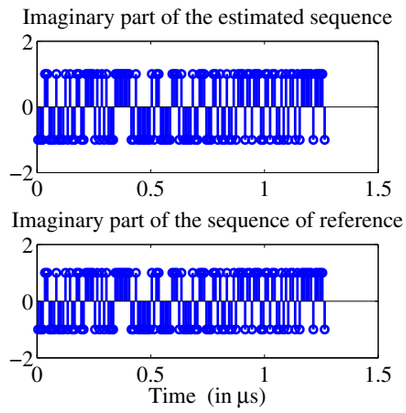


(d) Imaginary binary part of the code

Fig. 8. Spreading sequence estimation and *binarization*, SNR $= -7$ dB in uplink.

### 4.3 Spreading code and symbols estimation

The synchronization process leads to set $\alpha_0$=0, therefore, the correlation matrix becomes:

$$\mathbf{R}_{\alpha_0} = \sigma_b^2 \left\{ \beta \mathbf{v}_{\alpha_0} \mathbf{v}_{\alpha_0}^* + \mathbf{I} \right\}. \tag{28}$$

Equation 28 highlights a maximum eigenvalue which associated eigenvector contains the corresponding spreading sequence (excluding the effects of the global transmission filter), and $M-1$ eigenvalues (equal on average to the noise power at the receiver side). The largest eigenvalue corresponds to the eigenvector $\mathbf{v}_{\alpha_0}$, i.e., the signal spreading sequence (up to the channel effects).

The eigenvectors are calculated up to a complex multiplicative factor due to diagonalization. The complex factor effects are cancelled by normalizing the estimated eigenvector phase. It is made by maximizing its real part and imposing the positivity of its first component real part. In order to determine if the sequence whether initially complex or real, the variances of its real and imaginary parts (here $\mathbf{v}_{\alpha_0}$) after normalization are compared. The sequence is real when the standard deviation of its real part-to-the standard deviation of its imaginary part ration exceeds 2.5. This threshold seems to be sufficient because of eigenvectors normalization.

This stage allows us to eliminate the effects of the global transmission filter, as shown on Fig. 8 (a) and (b). The last stage is the *binarization* detailed in (Nsiala Nzéza, 2006). It consists in determining the chip period $T_c$ (hence the length of the sequences) before seeking the binary sequence the nearest to the spreading sequence estimated in the least squares sense for each of the sequences to be estimated, as highlighted on Fig. 8 (c) and (d).

## 5. Extension to the multiuser/multirate case

Starting with Equation 11, we will progressively extend to the multiuser/multirate case the blind methods developped in Section 4. The assumptions of independent, centered and noise-uncorrelated signals leads to the following equations:

$$\widehat{R}_{ss}(\theta) = \sum_{i=0}^{S-1} \sum_{n=0}^{N_u^i-1} \widehat{R}_{s_{n,i}s_{n,i}}(\theta), \text{ and } \widehat{R}_{yy}(\theta) = \widehat{R}_{ss}(\theta) + \widehat{R}_{bb}(\theta), \tag{29}$$

where $\widehat{R}_{s_{n,i}s_{n,i}}(\theta)$ and $\widehat{R}_{bb}(\theta)$ are the estimates of the $(n,i)^{th}$ noise-unaffected signal and that of the noise autocorrelation fluctuations, respectively. Indeed, since the fluctuations are computed from many randomly-selected windows, they do not depend on the signals relative delays $T_{d_{n,i}}$ nor on channel paths delays. The Multiple Access Interference (MAI) noise impact is similar to that of additive noise. So, as in single-user case, both MAI and Gaussian Additive noise fluctuations are uniformly distributed over the desired frequency band. Moreover, channel gains act as a multiplicative factor on fluctuations average amplitude.

Let us consider the channel-corrupted signal and the assumptions made in Section 2. Therefore, it is fairly easy to demonstrate that on average, high amplitudes of the fluctuations of the autocorrelation estimator, denoted $\Phi_s(\theta)$, are obtained for each $\theta$ multiple of each symbol period $T_{s_i}$, $i = 0, \cdots, S-1$. Since the symbol periods are different, let us denote $\Phi_i(\theta)$ the fluctuations of the autocorrelation estimator of the $N_u^i$ signals $s_{n,i}(t)$ transmitting at the same data rate $T_{s_i}$. Let us also term $m_{\Phi_i}$ the mean value of the fluctuations $\Phi_i(\theta)$ for each

value $\theta$ multiple of $T_{s_i}$; it leads to:

$$\Phi_i(\theta) = m_{\Phi_i} \cdot pgn_{T_{s_i}}(\theta), \tag{30}$$

where $pgn_{T_{s_i}}(\theta) = \sum_{k=-\infty}^{+\infty} \delta(\theta - kT_{s_i})$, and the function $\delta(\theta)$ is the KRONECKER function. Consequently, the signals being independent and centered by assumption, the fluctuations $\Phi_s(\theta)$ of the global noise-unaffected signal, for each value $\theta$ multiple of $T_{s_i}$, can be expressed as:

$$\Phi_s(\theta) = \sum_{i=0}^{S-1} \Phi_i(\theta) = \sum_{i=0}^{S-1} m_{\Phi_i} \cdot pgn_{T_{s_i}}(\theta). \tag{31}$$

Thus, theoretical calculations developed in Subsection 4.1.2 remain valid in this case, considering each group $i$ separately. Hence, the average amplitude of the fluctuations in each group $i$ becomes:

$$m_{\Phi_i} = \sum_{n=0}^{N_u^i-1} \frac{T_{s_i}}{T_F} \sigma^4_{s_{n,i}} = N_u^i \frac{T_{s_i}}{T_F} \sigma^4_{s_i} = N_u^i \frac{L_i T_c}{T_F} \sigma^4_{s_i}, \tag{32}$$

where $\sigma^4_{s_i} = \frac{1}{N_u^i} \sum_{n=0}^{N_u^i-1} \sigma^4_{s_{n,i}}$ can be considered as the average received power of signals within the group $i$. Equation 32 evidences that, the higher the number of users in a group $i$ is, the greater the average amplitude of the fluctuations due to signals within this group is. Then, let us set to $m_{\Phi_{snir}}$ both MAI and Gaussian Additive noise contribution to fluctuations. Therefore, the longer the sequence is, the higher the peaks of correlation fluctuations are, and the biggest amplitude is usually exhibited by the fluctuations of the users transmitting at the lowest data rate. This approach is a powerful tool to estimate symbol periods, and it allows to differentiate the various transmitted data rate and to distinguish between the different standards. As proved in (Nsiala Nzéza, 2006), their mean and standard deviation are given by:

$$\begin{aligned} m_{\Phi_{snir}} &= \frac{\sigma^4_{snir}}{WT_F} \quad \text{(a)}, \\ \sigma_{\Phi_{snir}} &= \sqrt{\frac{2}{M}} \frac{\sigma^4_{snir}}{WT_F} \quad \text{(b)}, \end{aligned} \tag{33}$$

where $\sigma^4_{snir}$ represents both MAI and Gaussian Additive noise power. Completing, using Equations 30, 31, 32 and 33, the global fluctuations can be expressed as follows:

$$\Phi(\theta) = \Phi_s(\theta) + \Phi_{snir}(\theta). \tag{34}$$

Equation 34 shows that the overall fluctuations are composed of fluctuations due to the signal and noise (Gaussaian additive and MAI). It also proves that only the contribution of the signal exhibits peaks at multiple of $T_{s_i}$ in each group $i$. The global fluctuactions curve highlights a superposition of regularly spaced peaks within each group $i$, while the noise is uniformly distributed in the band. As a result, within each group of $i$, the blind synchronization process can be performed, also allowing to determine the number of interfering users $N_u^i$ as detailed in Subsection . In addition, note that the impact of MAI noise becomes negligible if the interest first goes to peaks with the highest amplitude fluctuations (Nzéza et al., 2006), i.e., to signals transmitted at $\max_{i=0,\cdots,S-1} \{T_{s_i}\}$.

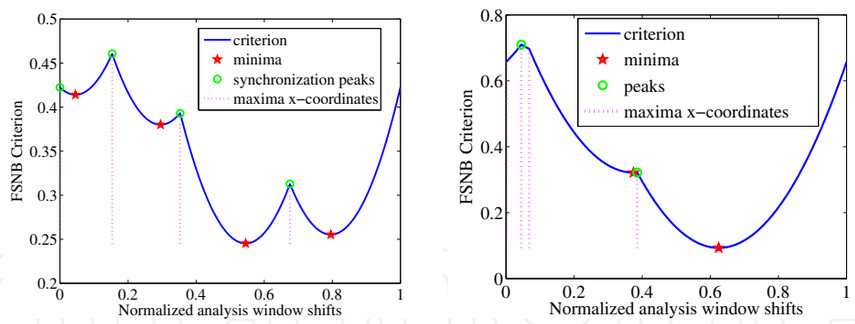


(a) ideal case (b) synchronization peaks masking

Fig. 9. Theoretical FSNB criterion $F$ in uplink for two cases.

### 5.1 Blind multiuser synchronization process

We first extend FSNB criterion to show that this criterion may exhibit the phenomenon of synchronisation peaks masking. Therefore, the modifed Pastd algorithm (Nsiala Nzéza, 2006)[pp. 115-116] may be jointly performed. Alternatively, we present another criterion based on the Maximum Eigenvalue Behaviour (MEVB) according to analysis window shifts. MEVB-based criterion provides a significant improvement of performances which is mainly due to suppression of synchronisation peaks masking that occurred with the FSNB criterion.

#### 5.1.1 FSNB criterion theoretical analysis

For more clearness, let us set $T_{s_i}{=}T_s$, $(*)_{n,i}{=}(*)_n$ within a group $i$. Since normalized shifts $\alpha_n$ restrict the study into the interval $[0, \quad 1[$, there is a periodicity on the relative positions of an analysis window and that of signals. By setting $\langle x \rangle \equiv \ x \ modulo \ 1$, $x \in \mathbb{R}$, $\tau_n = \frac{T_{d_n}}{T_s}$ and $d_f = \frac{D_f}{T_s}$, leads to $\alpha'_n = \langle d_f - \tau_n \rangle$, $n = 0, \cdots, N_u^i - 1$. Consequently, since delays $\tau_n$ are assumed constant, Equation 27 which only depends on shifts $d_f$ becomes:

$$F(d_f) = 1 + \sum_{n=0}^{N_u^i - 1} \{ \langle d_f - \tau_n \rangle^2 - \langle d_f - \tau_n \rangle \}. \tag{35}$$

Equation 35 shows that each signal is synchronized when $d_f$ is equal to its corresponding transmission delay. Let us recall that a peak is a point of a curve from which, while moving by lower or higher values, the curve is always decreasing. As well as synchronization peaks are expected at points $d_f = \tau_n$. This implies to examine criterion $F$ behaviour within $]\tau_{n-1}, \quad \tau_n]$ and $[\tau_n, \quad \tau_{n+1}[$. However for $n = 0$, or for $n = N_u^i - 1$, intervals $]\tau_{-1}, \quad \tau_0]$ and $[\tau_{N_u^i - 1}, \quad \tau_{N_u^i}[$ do not exist. Thus, by setting $\tilde{\tau}_n = \tau_{\langle n \rangle_{N_u^i}}$, $\quad \langle n \rangle_{N_u^i} \equiv n \ modulo \ N_u^i$ leads to take these intervals into account, and Equation 35 can be rewritten as:

$$F(d_f) = 1 + \sum_{n=0}^{N_u^i - 1} \{ \langle d_f - \tilde{\tau}_n \rangle^2 - \langle d_f - \tilde{\tau}_n \rangle \}. \tag{36}$$

Equation 36 is a convex quadratic function of $d_f$ over any interval $[\tilde{\tau}_n, \quad \tilde{\tau}_{n+1}[$ whose peaks should be located at points such that $d_f = \tilde{\tau}_n$, $n = 0, \cdots, N_u^i - 1$, as illustrated in Fig. 9 (a),

where $N_u^i = 4$, $\tilde{\tau}_0 = 0$, $\tilde{\tau}_1 = 0.1509$, $\tilde{\tau}_2 = 0.3784$ and $\tilde{\tau}_3 = 0.6979$. However, from Equation 36, we demonstrated that according to $\tilde{\tau}_n$, a local minimum of Equation 36 may not belong to the interval $[\tilde{\tau}_n \quad \tilde{\tau}_{n+1}[$; in this case, there could not be a synchronization peak at $d_f = \tilde{\tau}_n$: it is the phenomenon of synchronization peaks masking, as illustrated in Fig. 9 (b), with $\tilde{\tau}_0 = 0$, $\tilde{\tau}_1 = 0.0448$, $\tilde{\tau}_2 = 0.068$ and $\tilde{\tau}_3 = 0.3853$. By studying the behaviour of criterion $F$ in the vicinity of points such that $d_f = \tilde{\tau}_n$, leads to the finding of the following condition:

$$\tilde{\tau}_{n-1} < \frac{n}{N_u^i} < \tilde{\tau}_n < \frac{n+1}{N_u^i} < \tilde{\tau}_{n+1}. \tag{37}$$

Equation 37 gives the necessary and sufficient condition of the synchronization peaks existence, as proved in (Nsiala Nzéza, 2006). Although the masking of peaks phenomenon occurs if the timing offsets of multiple users are close to each other in an asynchronous system, the synchronization can however be achieved combining the process described above with the modified-Pastd algorithm (Nsiala Nzéza, 2006). Thus, this consideration led us to analyze the MEV-based (MEVB) criterion described hereinafter.

#### 5.1.2 MEVB criterion theoretical development

Without loss of generality, by setting $\sigma_b^2 = \beta = 1$ in Equation 24 leads to Equation 38, whose derivative with respect to the shift $d_f$ is given by Equation 39:

$$\begin{cases} \lambda_n^0 = 2 - \langle d_f - \tilde{\tau}_n \rangle \\ \lambda_n^{-1} = 1 + \langle d_f - \tilde{\tau}_n \rangle \end{cases} \text{(a)}, \quad \begin{cases} \lambda_{n+1}^0 = 2 - \langle d_f - \tilde{\tau}_{n+1} \rangle \\ \lambda_{n+1}^{-1} = 1 + \langle d_f - \tilde{\tau}_{n+1} \rangle \end{cases} \text{(b)}, \tag{38}$$

$$\begin{cases} \frac{\partial \lambda_n^0}{\partial d_f} = -1 < 0 \\ \frac{\partial \lambda_n^{-1}}{\partial d_f} = 1 > 0 \end{cases} \text{(a)}, \quad \begin{cases} \frac{\partial \lambda_{n+1}^0}{\partial d_f} = -1 < 0 \\ \frac{\partial \lambda_{n+1}^{-1}}{\partial d_f} = 1 > 0 \end{cases} \text{(b)}. \tag{39}$$

Equation 39 (a) shows that for any shift $d_f \in [\tau_n, \quad \tau_{n+1}[$, $\lambda_n^0$ decreases while $\lambda_n^{-1}$ increases, and conversely. The same result is obtained from Equation 39 (b), and the values for which they are equal are local minima. Therefore, the MEVB criterion is defined as the maximum value between two consecutive largest eigenvalues, which is equivalent to the following function $\mathcal{M}$:

$$\mathcal{M}(d_f) = \max_{\tau_n \leq d_f < \tau_{n+1}} \left( \lambda_n^0, \lambda_{n+1}^{-1} \right), \; n = 0, \cdots, N_u^i - 1. \tag{40}$$

Since eigenvalues are linear functions of $d_f$, Equation 40 always presents maxima, and synchronization peaks at $d_f = \tilde{\tau}_n$, contrary to the FSNB criterion, as illustrated in Fig. 10, with the same parameters as those used in Fig. 9 (b). Thus, this discussion highlights that the performances obtained by using the MEVB criterion will be better than those obtained by using the FSNB criterion, as it will be shown in Section 5.3. Let us note that both criteria can easily be derived for downlink transmissions by setting $\tau_n = 0$, $n = 0, \cdots, N_u^i - 1$ in all equations above. At last, the number of synchronization peaks gives the number of interfering users. A particular emphasis has to be placed on the FSNB criterion due to some masking peaks. Moreover, once all peak positions are known, the differences between their positions and the corresponding user for which the normalized shift is the closest to 0 or 1, give an estimation of the transmission delays.

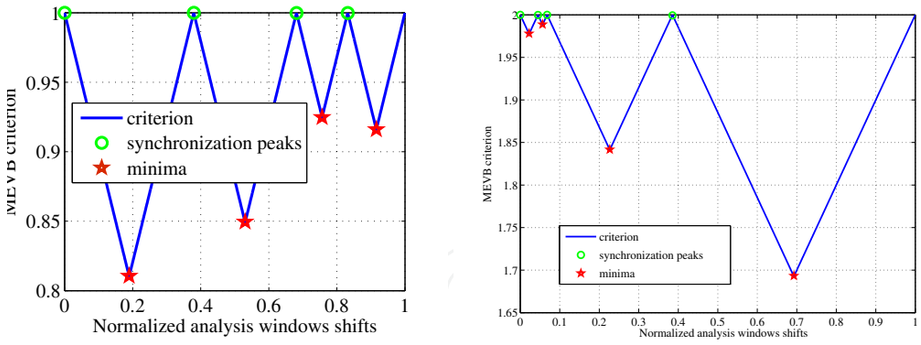


(a) ideal case (b) other cases

Fig. 10. Function $\mathcal{M}$ equivalent to the theoretical MEVB criterion in uplink, $N_u^i = 4$.

### 5.2 Sequences identification and symbols recovering

Once one of the interfering users within $i$ is synchronised in uplink, e.g., $d_f = \tau_0$, which corresponds to set $\alpha_0 = 0$, the correlation matrix becomes:

$$\mathbf{R} = \sigma_b^2 \left\{ \beta \left( \mathbf{v}_{\alpha_0} \mathbf{v}_{\alpha_0}^* + \sum_{n=1}^{N_u^i - 1} \left\{ (1-\alpha_n) \mathbf{v}_n^0 (\mathbf{v}_n^0)^* \alpha_n \mathbf{v}_n^{-1} (\mathbf{v}_n^{-1})^* \right\} \right) + \mathbf{I} \right\}. \tag{41}$$

Equation 41 highlights a maximum eigenvalue which associated eigenvector contains the corresponding spreading sequence (excluding the effects of the global transmission filter), and $2(N_u^i - 1)$ eigenvalues. Then, this process is performed in an iterative way so as to get the $N_u^i$ largest eigenvalues, which associated eigenvectors correspond to spreading sequences. In downlink, i.e., $\tau_n = 0$, $\alpha_n = \alpha$, $n = 0, 1, \cdots, N_u^i - 1$, the correlation matrix can be rewritten as:

$$\mathbf{R} = \sigma_b^2 \left\{ \beta \left( \sum_{n=0}^{N_u^i - 1} \left\{ (1-\alpha) \mathbf{v}_n^0 (\mathbf{v}_n^0)^* + \alpha \mathbf{v}_n^{-1} (\mathbf{v}_n^{-1})^* \right\} \right) + \mathbf{I} \right\}. \tag{42}$$

When users are synchronized, by using either the FSNB or the MEVB criterion, i.e., $\alpha = 0$, the induced corrlation matrix may be expressed as:

$$\mathbf{R} = \sigma_b^2 \left( \beta \sum_{n=0}^{N_u^i - 1} \mathbf{v}_n \mathbf{v}_n^* + \mathbf{I} \right). \tag{43}$$

Equation 43 exhibits the $N_u^i$ largest eigenvalues whose associated eigenvectors correspond to the spreading sequences, and the $M - N_u^i$ others are on average equal to the noise power. Finally, linear algebra techniques previously described in Section 4, applied to the estimated eigenvectors, allow to identify sequences used at the transmitter and to recover transmitted symbols.

### 5.3 Simulation results in the multiuser multirate case

Simulations were carried out with complex GOLD sequences of processing gains $L_0$=31 and $L_1$=127. The other parameters were set as follows. The common chip frequency $F_c$=100 MHz, the sampling frequency $F_e$=300 MHz, $T_F$=2$\mu s$, $K$=300, $N_u^0$=2, $N_u^1$=4, and thus $N_u$=6.

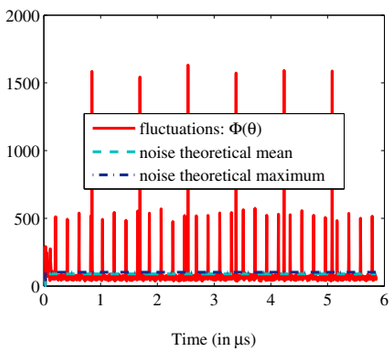


(a) Correlation fluctuations $\Phi(\tau)$

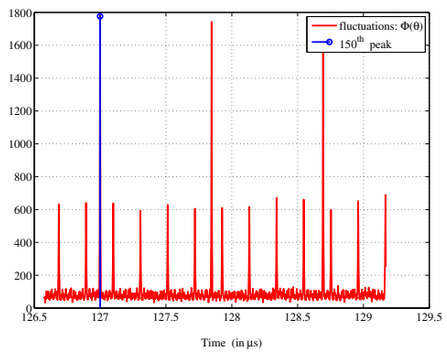


(b) Estimation of the symbol period $T_{s_1}$

Fig. 11. Estimation of the symbol period $N_u^0 = 2$, $N_u^1 = 4$, SNR$= -7$dB.

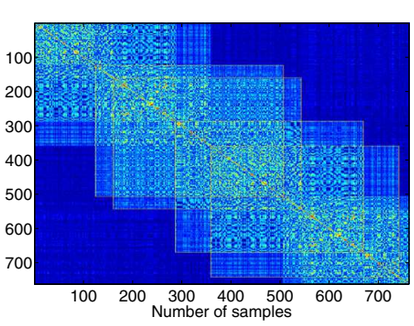


(a) Matrix $\mathcal{R}$ of double size before the sycnhronization

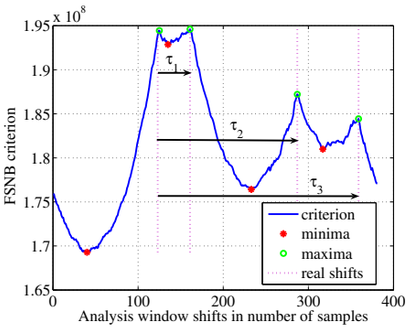


(b) Experimental FSNB criterion

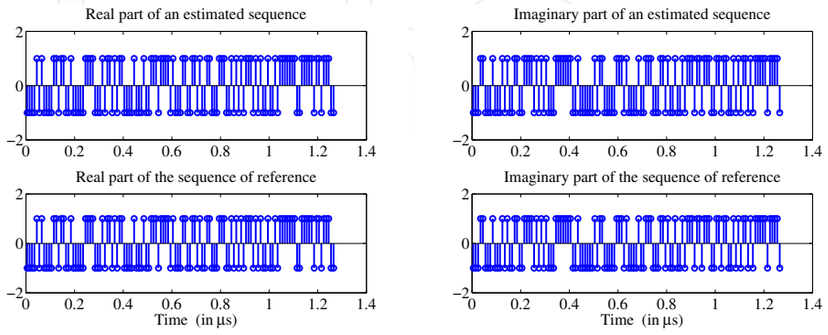


(c) Real and Imaginary parts of an estimated binary sequence

Fig. 12. Synchronization and sequences recovering, SNR$= -7$dB, $N_u^i = 4$, $L_1 = 127$.

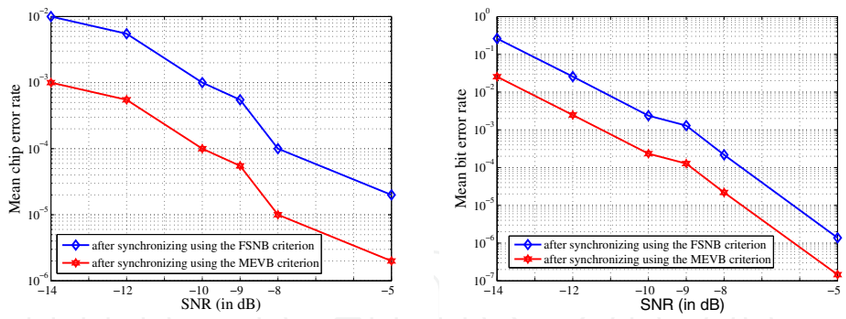


(a) Mean chip error rate (b) Mean bit error rate

Fig. 13. Both synchronization performances comparison for different SNRs, $N_u^1 = 4$, $L_1 = 127$.

A $QPSK$ modulation was considered in uplink. For the $N_u^1$ users, it was set $\alpha_0 = 0.3228$, $\alpha_1 = 0.4226$, $\alpha_2 = 0.7533$ and $\alpha_3 = 0.9423$. Fig. 11 (a) illustrates fluctuations of the correlation estimator $\Phi(\theta)$. The curve clearly highlights two sets of equispaced peaks of different amplitudes. This means that two sets of spread spectrum signals transmitting at two different rates are hidden in the noise. Estimated symbol periods, (in $\mu s$) are $\widetilde{T}_{s_0} = 0.31$, $\widetilde{T}_{s_1} = 1.27$. To re-estimate these values, for each set of autocorrelation fluctuations, let us look for a maximum near the farthest peak on the right side, e.g., the $100^{th}$ as shown in Fig. 11 (b), then we get $100 \times \widetilde{T}_{s_1} \approx 127 \mu s$.

Since symbol periods are available at this stage, e.g., $T_{s_1} = 1.27 \mu s$, the analysis window length is set as $T_F = T_{s_1}$. Fig. 12 (a) corresponding to the double size matrix $\mathcal{R}$ shows 4 overlapping matrices, suggesting that there are 4 interfering users. Matrix $\mathbf{R}$ before the synchronization corresponds to the $(M \times M)$-matrix extracted from $\mathcal{R}$. Fig. 12 (b) shows the experimental FSNB criterion calculated by moving along the diagonal of matrix $\mathcal{R}$ and calculating the squared norm of the shift-induced submatrix for each value of the shift. This squared norm will be maximum for the bright areas in Fig. 12 (a).

Fig. 12 (b) evidences 4 peaks which X-coordinates give the desynchronization times in number of samples. The number of peaks gives the number of active users over the analysis window, hence there are 4 interfering active users. By taking the oversampling factor into account, we obtain $\widehat{\alpha}_0 \approx 0.3281$, $\widehat{\alpha}_1 = 0.4226$, $\widehat{\alpha}_2 = 0.7533$ and $\widehat{\alpha}_3 = 0.9449$.

Since transmission delays and shifts are supposed to be sorted in the ascending order, the first peak, i.e., for $\widehat{\alpha}_0$, corresponds to the reference user. Thus, $\widehat{\tau}_1 = 0.0999$, $\widehat{\tau}_2 = 0.4252$, and $\widehat{\tau}_3 = 0.6221$. These values are very close to the real ones, and allow the synchronization of interfering users. Fig. 12 (c) shows the real and imaginary parts of one of the estimated sequences, which are equal to that used at the transmitter side, respectively.

Fig. 13 (a) highlights the performances in terms of mean chip error rate (MCER), i.e., the average ratio of the number of wrong sequence chips to the total number of sequence chips. It shows very low MCERs after synchronizing using either the MEVB or FSNB criterion. Moreover, MECRs obtained after using the MEVB criterion are lower than those obtained after using the FSNB one (with a 3 dB gain), in agreement with the theoretical analysis. It also shows that in average, one chip at most is wrong with sequences of length 127. Fig. 13 (b) shows the performances in terms of mean bit error rate (MBER). It clearly evidences very good

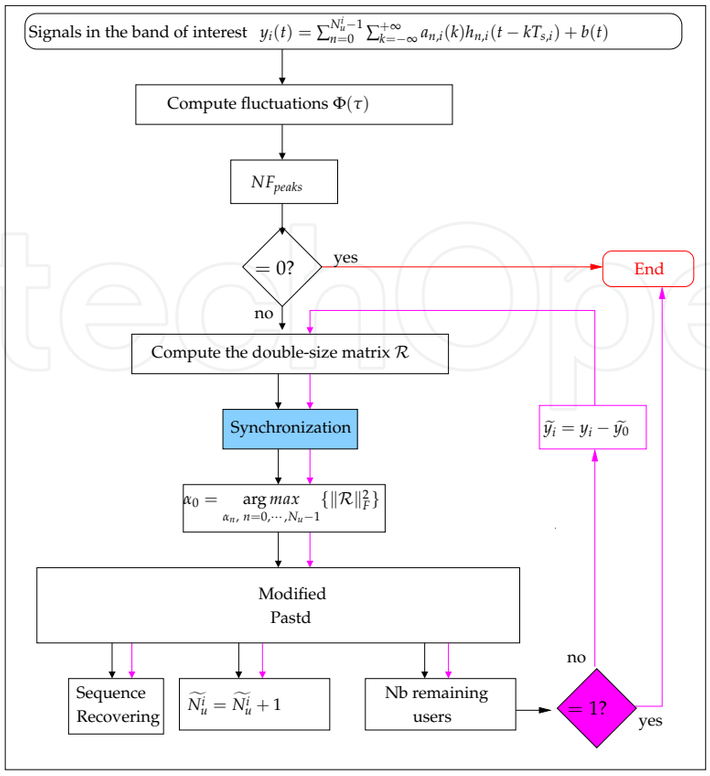


Fig. 14. Iterative implementation of the proposed scheme in the multiuser single rate case.

performances after synchronizing using both criteria and estimating transmitted symbols. In agreement with the results shown in Fig. 13 (a), lower MBERs are obtained ( with a 2 dB gain) after using the MEVB criterion. Typically, in some cooperative systems, the MBER is about $10^{-8}$ which is very close to that obtained at $-5$ dB after using the MEVB criterion.

## 6. Performances improvement of the proposed method

Note first that the overall chain is implemented in a way to make it interactive with an operator. As claimed in Section 3, although the proposed method has been described sequentially, the most efficient implementation of the three steps is to link them back iteratively. This allows the global chain performances improvement by deflating the estimated signal. This will be especially important when the number of interfering users within a given group of users transmitting at the same data rate increases, or when the differences between data rate from one group to another one is very high. In these cases, some synchronization peaks can be masked as proven in Section 5. Hence, it is advisable to adopt the iterative approach summarized on Fig. 14 and Fig. 15. Therefore, firstly identifying in the multiuser detection step the group of users corresponding to the largest sequence or fluctuations amplitude peaks, set to $NF_{peaks}$.

### 6.1 Implementation in the multiuser single rate case

This case is shown on Fig. 14. Within the identified group of users among $NF_{peaks}$, the user corresponding to the synchronization criterion maxima is first synchronized. Besides, the

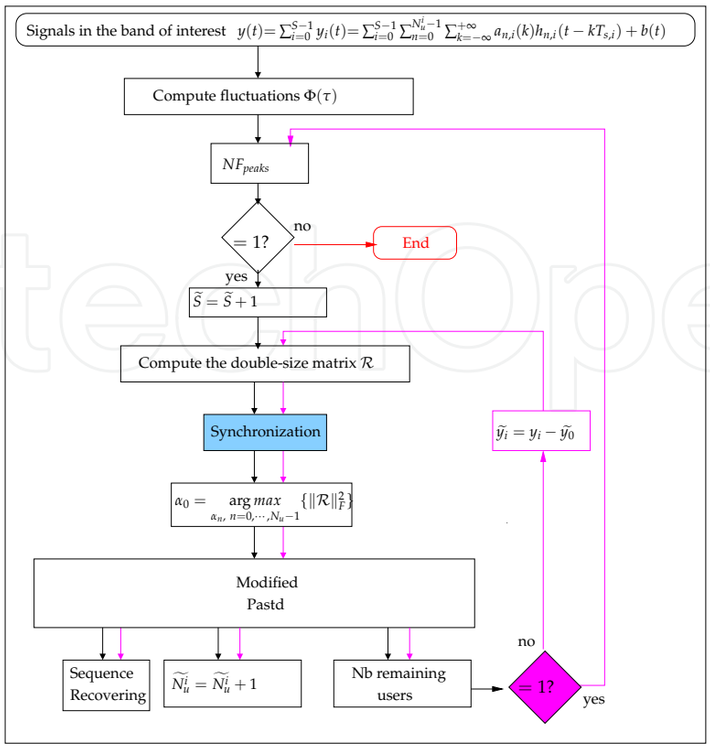


Fig. 15. Iterative implementation of the proposed scheme in multiuser multirate case

number of synchronization peaks set to $NS_{peaks}$ must be stored for further comparison in the algorithm. In the next step, the corresponding spreading sequences estimated will be the most reliable, since it will correspond to the eigenvector, thus the signal space associated with the largest eigenvalue.Ãl'At this stage, using the modified-Pastd algorithm aiming to estimate the number of users $\widetilde{N}_u^i$ is necessary.Ãl'The identified signal is substracted from the global signal corresponding to signals transmitted at the same data rate. Then, if the number of remaining users $Nb$ is not equal to one, the synchronization criterion may be computed again after the deflation, and the process is repeated as described on Fig. 14.

### 6.2 Implementation in the multiuser multirate case

The iterative implementation in the multiuser multirate context is illustrated on Fig. 15. In this case, first identify the group of users corresponding to the largest fluctuations amplitude peaks, and store the number $NF_{peaks}$ of group of fluctuations peaks. Then, the number of iteration compared to $NF_{peaks}$ is increased. Therefore, if $Nb \neq 1$, restart the process by selecting another group of fluctuations. Note that, improving the performances is achueved by recomputing the function $\Phi(\theta)$ after deflating the estimates of the signals whithin the identified group of interest.

### 6.3 Discussion and illustration through simulation results

In asynchronous multiuser multirate CDMA systems, the near-far effect is definitely present. Consequently, the multipath channels and/or under near-far effects may be mitigated through the iterative implementation of the proposed algorithms highlighted above. Indeed

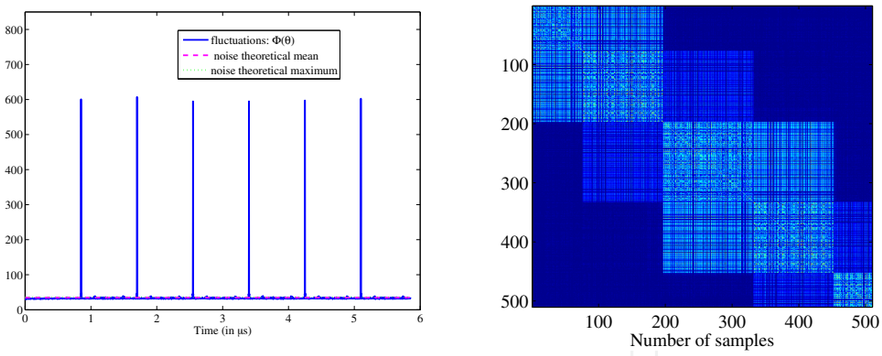


(a) Fluctuations $\Phi(\tau)$ (b) Double-size matrix $\mathcal{R}$

Fig. 16. Fluctuations and double-size correlation matrix analysis.

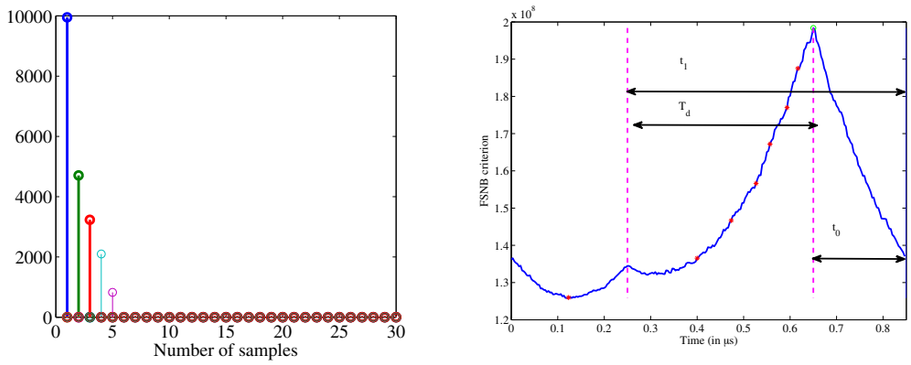


(a) Eigenvalues before the synchronization (b) Synchronization criterion

Fig. 17. Illustration of the synchronization process.

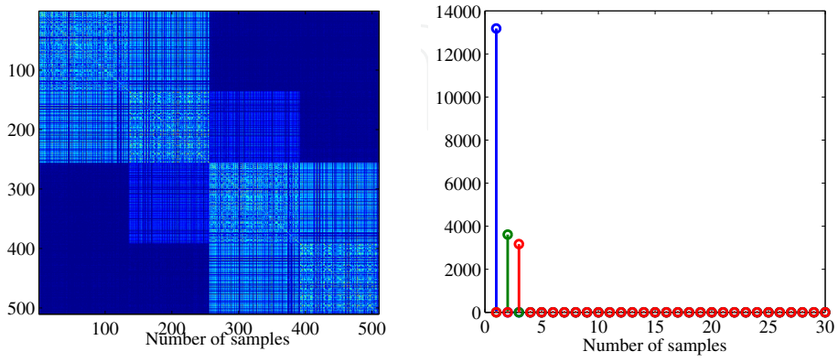


(a) Extracted matrix $\mathbf{R}_{\tilde{\alpha}_0}$ (b) Eigenvalues after the synchronization

Fig. 18. Illustration of the third step of the proposed scheme.

this iterative approach jointly uses the modifed-Pastd algorithm and a feedback on either synchronization criteria or fluctuations of correlation estimators computation. Besides, note that the deflation technique is widely used in CDMA signals detection in both blind and cooperative methods. The originality of our approach lies in the analysis of the fluctuations of correlation estimators, and in the synchronization criteria implemented.

As a result, the proposed algorithms may be applied to the long sequence code case, as investigated in Section 7 through simulation results.

Let us now illustrate the iterative implementation using the FSNB criterion with following simulations parameters were set: $N_u^0 = 2$ complex GOLD sequences of processing gain $L_{0,0} = L_{1,0} = 255$, with inequal powers: $\sigma_{s_0}^2 = 1$ and $\sigma_{s_1}^2 = 0.5022$, $\sigma_b^2 = 5.3307$, $F_c = 300$ MHz, $F_e = 600$ MHz, $T_F = 2\mu s$, $K = 894$, a $QPSK$ modulation was considered in uplink. For the $N_u^0$ users, it was set $t_0 = 0.2\ \mu s$, $t_1 = 0.6\ \mu s$, $\text{SNR}_0 = -6.3$ dB, $\text{SNR}_1 = -9.78$ dB, what leads to a global SNR$\simeq -11$ dB at the receiver side. From Fig. 16 (a), we get $\widetilde{T_S} = 0.85\ \mu s$, which allows to compute the double-size matrix $\mathcal{R}$, as shown on Fig. 16 (b). Even though on Fig. 16 (a), an estimation was not possible for $N_u^0$, the analysis of Fig. 16 (b) suggests that there could be $\widetilde{N}_u^0 = 2$ two users.

This is also reinforced by the eigenvalue decomposition that reveals 4 largest eigenvalues, as illustrated on Fig. 17 (a). However, the synchronization criterion on Fig. 17 (b) exhibits only one peak, from which we get $\widetilde{t_0} = 0.208$, and the estimates $\widetilde{T_d} = 0.342\ \mu s$. The EVD on Fig. 17 (b) of the corresponding extrated matrix $\mathbf{R}_{\widetilde{\alpha}_0}$ on Fig. 18 (a) exhibits 3 largest eigenvalues as expected. Since the use of the modified-Pastd algorithm leads to $\widetilde{N}_u^0 = N_u^0$, the contibution of the estimated signal is substracted from the global received signal and we continue by recomputing the criterion in order to estimate the second user.

Computing again another double-size matrix as shown on Fig. 19 (a). Its EVD on Fig. 19 (b) leads to only two largest eigenvalues as expected. Besides, the obtained criterion in this second iteration on Fig. 20 (a) exhibits only one synchronization peak, which allows to synchronize the corresponding user. Furthermore, the sequence recovering process may be performed, starting with the eigenvector corresponding to the remaining largest eigenvalue as shown on Fig. 20 (b).

## 7. Application to long spreading sequences transmission case

In order to clear up the reader, the application of the proposed method will be done through simulations in uplink. The multiuser case can be easily deduced as it will be further shown. Following parameters were set: Complex GOLD sequence of Length $L_0$=63, $Q_s$=3 which implies $Q_s T_s = LT_c$ (see Subsection 2.1.2 for details), $BPSK$ modulation $\alpha_0$=0.2, $F_e$=300 $MHz$, $F_c$=150 $MHz$, $T_F$=2 $\mu s$,$K$=666, SNR $= -3$ dB. Fig. 21(a) illustrates double-size matrix $\mathcal{R}$ computed with the estimates $Q_s * \widetilde{T_S}$=1.20 $\mu s$ in this case. The fluctuations curve is not represented here since it the same as in the short code case. The great difference is in estimating $Q_s * \widetilde{T_S}$=1.2588 $\mu s$ rather than $\widetilde{T_S} = L/F_c$=0.42 $\mu s$, and we get $\widetilde{\alpha}_0$=0.1667 which is very close to the real value. Seeing $2 * Q_s$=6 overlapping subspaces as expected. Compared to the short code case,i.e., $Q_s$=1, obtaining $2 * Q_s$=2 overlapping subspaces, as detailed in Section 4.

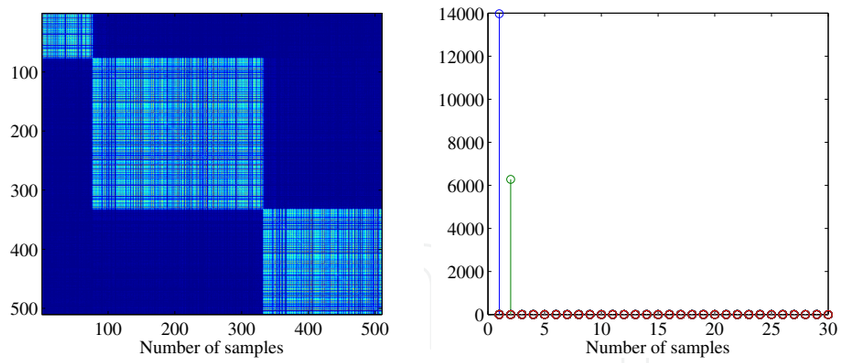


(a) Double-size matrix $\mathcal{R}$ (b) Eigenvalues before the synchronization

Fig. 19. Subspace analysis before the synchronization process in the second loop after deflation.

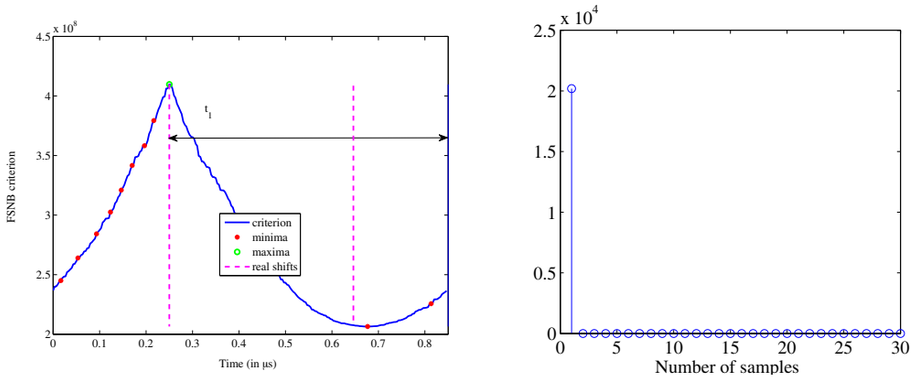


(a) Synchronization criterion (b) Eigenvalues after the synchronization

Fig. 20. Synchronization process in the second loop after deflation.

Besides, the criterion synchronization on Fig. 21 (b) proves that there are $Q_s$=3 subspaces corresponding to the $Q_s$=3 part of the spreading sequence. Therefore, synchronizing starting from the criteria maximum allows the extraction of the corresponding sub-matrix as indicated on Fig. 21 (c), on which linear algebra techniques application described in Section 4 lead to the estimation of a part the spreading sequence. The process is done $Q_s-1$ times in order to estimate the whole spreading code as depicted on Fig. 21 (d).

To complete, in the multiuser context, theoretical developments in Section 5 remain valid for the long case. Indeed, let us have a look on Fig. 22 obtained with the same parameters than on Figures 16 and 17, but with $Q_s$=5 for the two users ($N_u^0$=2). As evidenced on Fig. 22 (a) $N_u^0 * 2 * Q_s$=20 overlapping subspaces, which suggests that there are two interfering users with long spreading codes. However, $(N_u^0-1)*2*Q_s$=10 overlapping subspaces are not very remarkable as they correspond to the user received with a very low power. This is confirmed by the synchronization criterion plotted on Fig. 22 (b) which only emphasizes the shifts of the signal received with the highest power, i.e., the equispaced maxima of all the synchronization maxima. Fig. 22 (b) highlights the synchronization peaks masking. Hence,

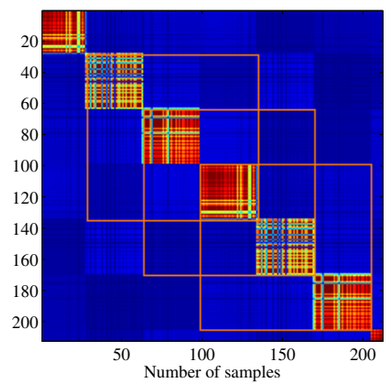


(a) Double-size matrix $\mathcal{R}$

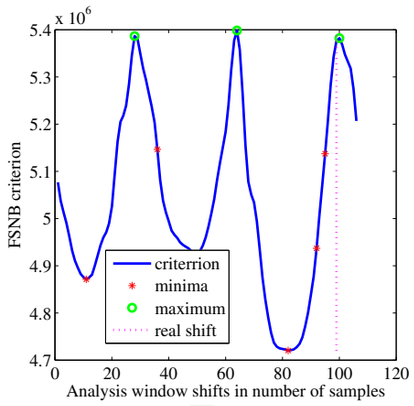


(b) Synchronization criterion

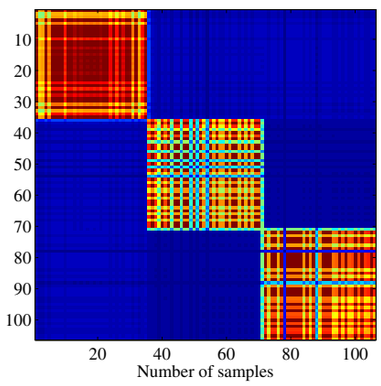


(c) Extracted matrix **R**

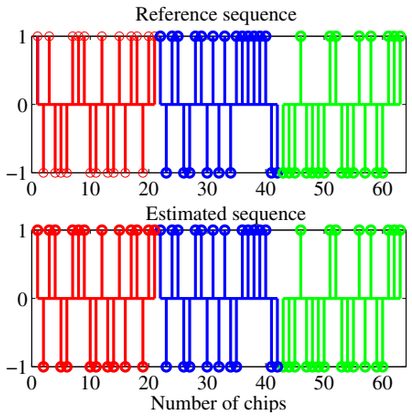


(d) Sequence estimation after *binarization*

Fig. 21. Application of the proposed algorithm to the single user long code case in uplink.

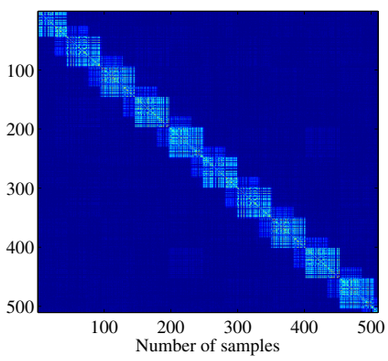


(a) Double-size matrix$\mathcal{R}$

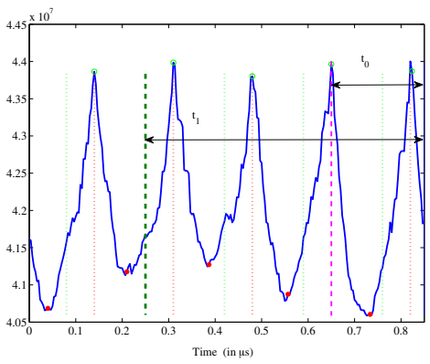


(b) Synchronization criterion

Fig. 22. Illustration of the synchronization process with $N_u^0 = 2$ users in uplink.

the process described above for the case on Fig. 21 may be performed in order to recover the corresponding spreading sequences for this user. Furthermore, after the deflation of the user

as we just estimated, and recomputing the synchronization criterion in order to estimate the second interfering user as depicted in Subsection 6.3.

## 8. Chapter summary and conclusion

In this chapter, we described a fast and efficient blind spread spectrum signal analysis approach consisting on signal detection, synchronization and identification of all concomitant data rates and user's sharing the same bandwidth in DS-CDMA transmissions. All this signal processing bricks are dedicated to the self-reconfiguration of Cognitive Radio terminals. We have evidenced that this approach permits to differentiate various CDMA standards through the assessment of interfering signals data rate. The methods and algorithms we have developed for these three steps allow to determine CDMA signals parameters: number of standards or rates, number of users for each rate, type of long or short sequences, the resynchronization time, spreading sequences and to despread signals of each user. We have shown that even in a sequential implementation,the approach developed and implemented here is very efficient both in terms of detection, synchronization and identification. Moreover, its performances improvement has been addressed thourgh two synchronization criteria. The first one has a very low computational cost and the second one permit to greatly reduce the phenomenon of peak masking, related to resynchronization times too close or excessive power difference between two users. Alternatively, a proposed iterative implementation that can suppress almost all the problems of peak masking by successive subtractions of interfering users was detailed. From which, short or long codes DS-CDMA signals blind detection and identification may be performed. Finally, the major part of the signal processing block of this approach were implemented on an operational system for the monitoring of radio frequency spectrum.

## 9. References

Buzzi, S., Venturino, L., Zappone, A. & Maio, A. D. (2010). Blind user detection in doubly dispersive ds/cdma fading channels, *IEEE Transaction on Signal Processing* 58(3): 1446–1451.

Cheraghi, P., Ma, Y. & Tafazolli, R. (2010). A novel blind spectrum sensing approach for cognitive radios, *PGNET 2010 Conference*, Marrakech, Morroco.

Committee, C. . M. (1989). *Digital land mobile radio communications : final report*, Euratom publications - EUR 12160 EN, Information technologies and sciences, *Commission of the European Communities*.

Ghavami, S. & Abolhassani, B. (2008). Blind chip rate estimation in multirate cdma transmissions using multirate sampling at slow flat fading channels, *IEEE ICCS 2008*, Singapore, pp. 1344– 1348.

Ghavami, S. & Abolhassani, B. (2009). On the performance of blind chip rate estimation in multi-rate cdma transmissions using multi-rate sampling in slow flat fading channels, *Wireless Sensor Network* 2: 67–75.

Hosseini, S., H, A. & J.A., R. (2010). A new cyclostationary spectrum sensing approach in cognitive radio, *IEEE SPAWC*, Marrakech, Morroco, pp. 1–4.

Khodadad, F. S., Ganji, F. & Mohammad, A. (2010). A practical approach for coherent signal surveillance and blind parameter assessment in asynchoronous ds-cdma systems in multipath channel, *Iranian Conference on Electrical Engineering*, Isfahan, Iran, pp. 305–310.

Khodadad, F. S., Ganji, F. & Safaei, A. (2010). A robust pn length estimation in down link low- snr ds-cdma multipath channels, *IEEE International Conference on Advanced Communication Technology* , Angwon-Do, South Korea, pp. 951–955.

Kibangou, A. Y. & de Almeida, A. (2010). Distribured parafac based ds-cdma blind receiver for wireless sensor networks, *IEEE SPAWC*, Marrakech, Morroco, pp. 1–5.

Koivisto, T. & Koivunen, V. (2007). Blind despreading of short-code ds-cdma signals in asynchronous multi-user systems, *Signal Processing (87)* 87(11): 2560–2568.

Meng, Y., You, M.-L., Luo, H.-W., Liu, G. & Yang, T. (2010). The linearly constrained lscma for blind multi-user detection, *Wireless Personal Communications: An International Journal* 53(2): 199–209.

Mitola, J. (2000). *Cognitive Radio: An Integrated Agent Architecture for Software Defined Radio*, PhD thesis, Royal Institute of Technology (KTH), Stockholm, Sweden.

Nsiala Nzéza, C. (2006). *Récepteur Adaptatif Multi-Standards pour les Signaux à Étalement de Spectre en Contexte Non Coopératif*, PhD thesis, Université de Bretagne Occidentale, Brest, France.

Nsiala Nzéza, C., Gautier, R. & Burel, G. (2004). Blind synchronization and sequences identification in cdma transmissions, *IEEE-AFCEA-MilCom*, Monterey, California, USA.

Nzéza, C. N., Gautier, R. & Burel, G. (2006). Blind Multiuser Detection in Multirate CDMA Transmissions Using Fluctuations of Correlation Estimators, *IEEE Globecom 2006*, San Francisco, California, USA, pp. 1–5.

Nzéza, C. N., Gautier, R. & Burel, G. (2008). Theoretical Performances Analysis of the Blind Multiuser Detection based on Fluctuations of Correlation Estimators in Multirate CDMA Transmissions, *Military Technical Academy Journal*.

Nzéza, C. N., Moniak, G., Berbineau, M., Gautier, R. & Burel, G. (2009). Blind MC-DS-CDMA parameters estimation in frequency selective channels, *IEEE-GlobeCom-5th IEEE Broadband Wireless Access Workshop*, Honolulu, Hawaii, USA.

Shen, L., Wang, H. & andZhijin Zhao, W. Z. (2011). Blind spectrum sensing for cognitive radio channels with noise uncertainty, *IEEE Transaction on Wireless Communications* 10(6): 1721–1724.

Williams, C., Beach, M., Neirynck, D., A. Nix, K. C., Morris, K., Kitchener, D., Presser, M., Li, Y. & McLaughlin, S. (2004). Personal area technologies for internetworked services, *IEEE Communication Magazine* 42(12): 15–32.

Yu, M., Chen, J., Shen, L. & Li, S. (2011). Blind separation of ds-cdma signals with ica method, *Journal of Networks* 6(2): 198–205.

Zhang, T., Dai, S., Zhang, W., Ma, G. & Gao, X. (2011). Blind estimation of the pn sequence in lower snr ds-ss signals with residual carrier, *Digital Signal Processing In Press* .


**Advances in Cognitive Radio Systems**

Edited by Dr. Cheng-Xiang Wang

ISBN 978-953-51-0666-1
Hard cover, 150 pages
**Publisher** InTech
**Published online** 05, July, 2012
**Published in print edition** July, 2012

**How to reference**

In order to correctly reference this scholarly work, feel free to copy and paste the following:

Crepin Nsiala Nzeza and Roland Gautier (2012). Blind Detection, Parameters Estimation and Despreading of DS-CDMA Signals in Multirate Multiuser Cognitive Radio Systems, Advances in Cognitive Radio Systems, Dr. Cheng-Xiang Wang (Ed.), ISBN: 978-953-51-0666-1, InTech, Available from: http://www.intechopen.com/books/advances-in-cognitive-radio-systems/blind-detection-parameters-estimation-and-despreading-of-ds-cdma-signals-in-multirate-multiuser-cogn

INTECH
open science | open minds

**InTech Europe**
University Campus STeP Ri
Slavka Krautzeka 83/A
51000 Rijeka, Croatia
Phone: +385 (51) 770 447
Fax: +385 (51) 686 166
www.intechopen.com

**InTech China**
Unit 405, Office Block, Hotel Equatorial Shanghai
No.65, Yan An Road (West), Shanghai, 200040, China
中国上海市延安西路65号上海国际贵都大饭店办公楼405单元
Phone: +86-21-62489820
Fax: +86-21-62489821

IntechOpen